Singlet oxygen-based photoelectrochemical detection of DNA

Saranya Thiruvottriyur Shanmugam[a, b], Stanislav Trashin[a, b], Karolien De Wael[a, b*]

[a]*A-Sense Lab, Department of Bioengineering, University of Antwerp, Groenenborgerlaan 171, 2020 Antwerp, Belgium.*

[b]*NANOlab Center of Excellence, University of Antwerp, Groenenborgerlaan 171, 2020 Antwerp, Belgium*

[*]*Corresponding author, karolien.dewael@uantwerpen.be*

Abstract

The current work, designed for the photoelectrochemical detection of DNA, evaluates light-responsive DNA probes carrying molecular photosensitizers generating singlet oxygen ($^1O_2$). We take advantage of their chromophore's ability to produce $^1O_2$ upon photoexcitation and subsequent photocurrent response. Type I, fluorescent and type II photosensitizers were studied using diode lasers at 406 nm blue, 532 nm green and 659 nm red lasers in the presensce and absence of a redox reporter, hydroquinone (HQ). Only type II photosensitizers (producing $^1O_2$) resulted in a noticeable photocurrent in 1-4 nA range upon illumination, in particular, dissolved DNA probes labeled with chlorin e6 and erythrosine were found to give a well-detectable photocurrent response in the presence of HQ. Whereas, Type I photosensitizers and fluorescent chromophores generate negligible photocurrents (< 0.15 nA). The analytical performance of the sensing system was evaluated using a magnetic beads-based DNA assay on disposable electrode platforms, with a focus to enhance the sensitivity and robustness of the technique in detecting complementary DNA targets. Amplified photocurrent responses in the range of 70-100 nA were obtained and detection limits of 17 pM and 10 pM were achieved using magnetic beads-captured chlorin e6 and erythrosine labeled DNA probes respectively. The presented novel photoelectrochemical detection can further be optimized and employed in applications for which enzymatic amplification such as polymerase chain reaction (PCR) is not applicable owing to their limitations and as an effective alternative to colorimetric detection when rapid detection of specific nucleic acid targets is required.

Keywords: Photoelectrochemistry; singlet oxygen; nucleic acids; DNA detection

1. Introduction

Detection of specific DNA and RNA sequences has a great potential in clinical diagnostics including the detection of pathogens (Li et al. 2021; Niemz et al. 2011), the diagnosis of genetic diseases (Rahat et al. 2020), and the detection of markers for different malignancies (Bronkhorst et al. 2020) and other clinical pathologies (Bhargava et al. 2017; Sfragano et al. 2021). Thus, many researchers have attempted to develop analytical strategies to facilitate point-of-care DNA detection and have elaborated multiple platforms with or without PCR amplification (Kim et al. 2021). Electrochemical sensors have become one of the most promising platforms due to technological advances in microelectronics, high sensitivity of electrochemical methods and commercial availability of low-cost disposable electrodes used as the sensor

transducer (Ferapontova 2018; Rashid and Yusof 2017; Santhanam et al. 2020; Thiruvottriyur Shanmugam et al. 2020).

Since oligonucleotides exhibit poor and irreversible intrinsic electrochemistry due to oxidation at large overpotentials, the use of attached or intercalated redox labels was introduced (García-González et al. 2014; Kokkinos 2019). However, the electrochemical activity of such electroactive labels and indicators strongly depends on their distance to the electrode surface due to a major potential drop in the electrical double layer (*ca.* 1 nm). Thus, the orientation of hybridized duplexes, their dynamics on the surface, and backfilling or contamination of the unoccupied surface affect the electrochemical response in a complex manner and may result in poorly reproducible data. For this reason, the use of enzymatic labels generating an electroactive product stays the most prominent analytical strategy (Liu et al. 2020; Wang et al. 2020).

In contrast to redox and enzymatic labels, fluorescent labels have become a routine tool in bioanalysis and biochemical research. The variety in their excitation spectra covering the visible range made multiplexing possible in the analysis, while high extinction coefficients and fluorescence quantum yields ensured high sensitivity. However, fluorescent dyes are often prone to photobleaching due to the formation of reactive oxygen species (ROS) due to side reactions (Demchenko 2020). Nevertheless, the labels with a high tendency to form ROS have found applications in electron microscopy (Malatesta et al. 2012) and biochemical research for local damaging (ca. 1 nm distance) of biomolecules and cellular components by highly reactive hydroxyl radicals (Horaková-Brazdilova et al. 2008). Such light-responsive fluorescent labels combine the high specificity of biomolecules (DNA or antibody) and photosensitizing properties of the dyes. Despite the variety in known fluorescent probes, oligonucleotides labeled by photosensitizers and their applications in (Photo)electrochemistry are scarcely represented in the literature.

Previously, we demonstrated the photoelectrochemical detection of a specific oligonucleotide linked to pheophorbide a, a photosensitizer known to generate singlet oxygen ($^1O_2$) under red light illumination (Trashin et al. 2017). However, large lipophilic labels may show steric hindrance due to aggregation leading to a lower coupling yield, potentially impacting the properties of oligonucleotides. A more systematic study is needed to explore the photoelectrochemical detectability of the light-responsive DNA probes carrying molecular photosensitizers. Nevertheless, photoelectrochemical sensors for DNA detection were extensively reported in the literature (Zhao et al. 2014b). All of them were based on photoinduced electron-transfer reactions (mostly in semiconducting or conducting nanoparticles used as

labels (Victorious et al. 2021) or changes in photocurrent of underlying photoelectroactive polymers or complex composite coatings (Liu et al. 2018; Tokudome et al. 2005; Wang et al. 2014).

In this work, we have studied a series of generally known light-responsive DNA probes (DNA sequence labeled with chromophores) to assess their ability to generate a photocurrent upon illumination. More specifically we have chosen commercially available chromophores linked to DNA with absorbance maxima nearly matching the wavelengths of commonly available diode laser pointers (405, 532 and 659 nm). Then the detectability of these DNA probes was assessed in different settings, such as (i) surface captured, via hybridization to the surface-confined complementary capture DNA probe (attached to the electrode surface via the thiol group), (ii) dissolved, in measuring solutions and (iii) captured at the surface of magnetic beads, via hybridization to the complementary capture DNA probe attached to the beads, to correlate the observed photocurrent with their properties to better understand the underlying molecular mechanisms.

2. Experimental

2.1 Chemicals

Chlorin e 6 (ChlE6, purity ≥ 98%, Cayman chemical company, USA), methylene blue (MetB, Reag. Ph Eur, Merck KgaA, Germany), malachite green (MalG, purity ≥ 96%, J&K Scientific, Belgium) eosin Y (EosY, purity ~ 99%, Sigma Aldrich), erythrosin B (EryB, purity ≥ 95%, Merck Schuchardt OHG), ATTO 532 (Eurogentec, Belgium), Rose Bengal (RB, purity >95%, Sigma-Aldrich), quinacrine (purity > 90%, Sigma Aldrich), hydroquinone (HQ, Acros Organics, Belgium) were used as received.

DNA modified at 5'-end by the chromophores (Fig. 1) were synthesized and purified by Eurogentec (Belgium) except DNA-MetB which was prepared by Metabion (Germany). The structures and purity were confirmed by mass spectrometry by the supplier. The DNA sequence 5'-TCA-ACA-TCA-GTC-TGA-TAA-GCT-A 3' was chosen to be complementary to microRNA-21 (miR-21), an important marker for several types of cancer and cardiovascular diseases (Tavallaie et al. 2015). The chromophores were attached to DNA via a 5' amino-C6 linker using either activated carboxylic or isothiocyanate functionality. The acridine derivative was used as phosphoramidite and was attached via direct link extension. Complementary (5' TAG-CTT-ATC-AGA-CTG-ATG-TTG-A-3') and scrambled non-complementary (5' TAG-CTT-ATG-TGT-ACC-CTG-TCA-G-3') DNA were modified at 5'-end by thiol C6 (HS-$(CH_2)_6$-) or Biotin TEG (a 16-atom spacer based on a triethylene glycol) by Eurogentec (Belgium) for immobilization on gold and streptavidin-modified surfaces, respectively.

4
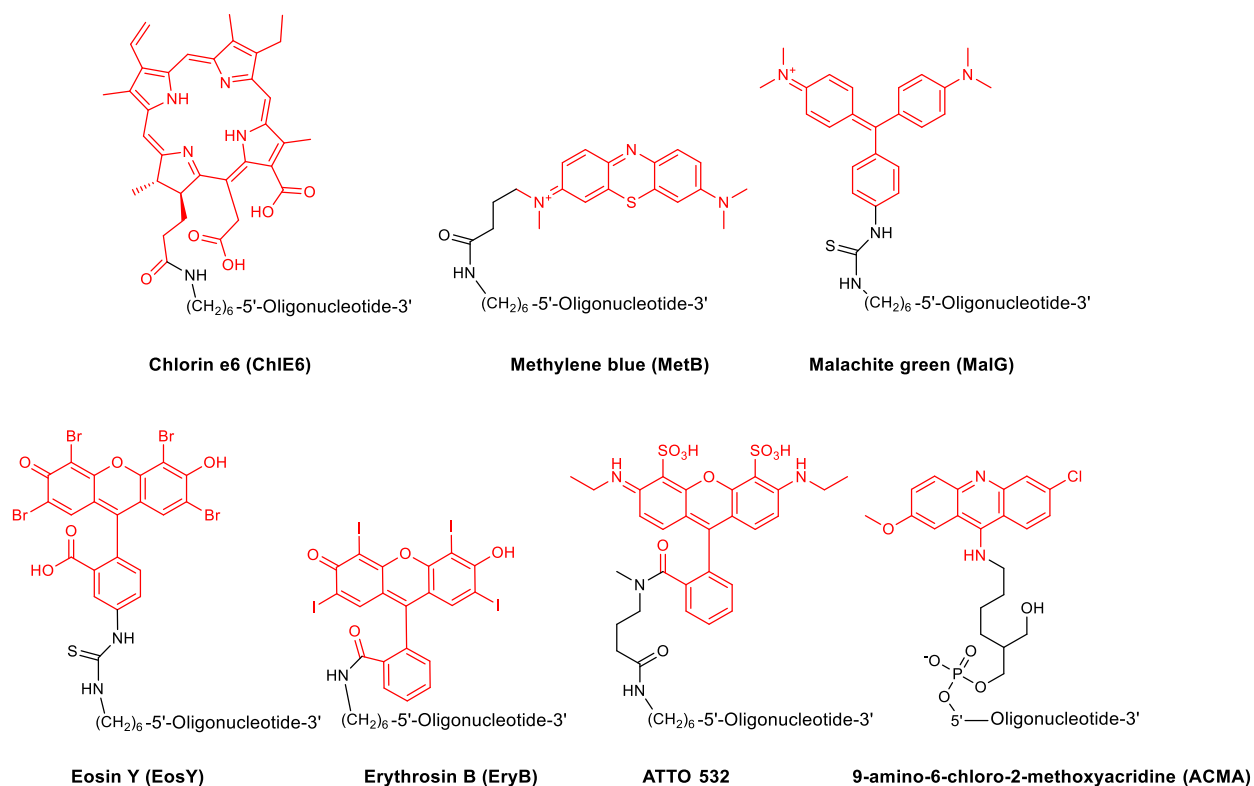
Figure 1. Structures of chromophores attached to DNA used in this study.

2.2 Preparation of gold disk electrodes

The gold disk electrodes (1.6 mm diameter, BASi®, USA) were polished with diamond spray (3, 1, 0.25 µm from Struers) and alumina slurry (0.05 µm from SPI supplies) and cleaned after each step in pure ethanol and MQ water in an ultrasonic bath. Following this, the electrodes were cleaned electrochemically by cyclic voltammetry in 0.5 M NaOH (between −0.35 and −1.4 V versus SCE) and then in 0.5 M H_2SO_4 (between 0.25 V to 1.5 V versus SCE at 0.1 V/s) until repeatable voltammograms were obtained. Freshly prepared electrodes were incubated in 1 µM thiolated capture DNA probe containing 0.2 µM mercaptohexanol (MH, purity >98.0%, TCI chemicals) in immobilization buffer overnight (~16 hours) and then in 1 mM MH for 2 h, for backfilling and removing weakly bound DNA molecules. For the hybridization step, a 40 µL drop of labeled DNA was placed on the electrode for 1 h and washed with a copious amount of wash buffer. Immobilization (Tris) buffer contained 500 mM KCl, 50 mM $MgCl_2$, and 10 mM Tris pH 7.5. The wash buffer (Tris-T20) had the same composition but additionally contained 0.05% w/v tween 20.

2.3. DNA immobilization on magnetic beads

5

A fraction (10 µl of the stock suspension per one measurement) of streptavidin modified magnetic beads (Dynabeads® M-280 Streptavidin, 10 mg/mL, Invitrogen) was washed three times with PBST20 (0.05% Tween 20 in PBS pH 7.4 buffer containing 10 mM Na_2HPO_4, 137 mM NaCl, 1.8 mM KH_2PO_4 and 2.7 mM KCl). Then they were incubated with 0.5 mL 1 µM biotinylated complementary or non-complementary sequences in PBST20 on a thermal shaker at 37°C, 250 rpm for 1 hour. Next, they were washed and incubated with the labeled DNA on a thermal shaker at 37°C, 250 rpm for 1 hour. Finally, the beads were washed two times with PBST20 and another wash with PBS and stored in PBS before measurements.

2.4. Photoelectrochemical measurements

Photoelectrochemical measurements were carried out with a µAutolab III (Metrohm-Autolab BV) using Nova 1.11 software. Diode lasers operating at 659 nm, 532 nm and 405 nm were purchased from Roithner Lasertechnik (Austria). The light power was adjusted to 30 mW using a light power meter (Thorlabs, Inc.). The diameter of the light beam was adjusted to illuminate the working electrodes. The on/off switch for illumination was preprogrammed and controlled by an Arduino Uno equipped with a relay. The background electrolyte used for all measurements consisted of 0.1 M KCl and 0.01 M KH_2PO_4 adjusted to pH 7 (phosphate buffer) providing same ionic strength for all measurements. HQ solutions used for measurements were prepared in this phosphate buffer and stored in icebath until measurements.

Three electrochemical setups were used for photoelectrochemical measurements (Fig. 2). Setup 1 was made of an open vessel containing 10 mL of electrolyte with a working gold disk electrode inserted from the bottom for illumination with light. An SCE reference (SCE, radiometer, Denmark) and platinum wire counter electrodes were placed in solution from the top. Measurements were conducted at a potential of –0.05 V vs. SCE. Setup 2 was introduced to minimize the amount of working solution required per experiment. A drop of 80 µL was placed on the gold disk electrode oriented upwards. Then a screen-printed electrode (SPE, IS-C, ItalSens) covered the drop from the top that the SPE reference and counter electrodes of the SPE were immersed in the measuring solution. A hole of 2 mm in diameter was preliminarily punctured in the place of the SPE working electrode (which is not used in the measurements) for illumination with the lasers. The difference of 90 ± 3 mV between the potential of the SCE and the

6

quasi silver SPE reference electrode was considered (−0.14 V vs the SPE reference electrode was applied) to reproduce conditions in Setup 1.
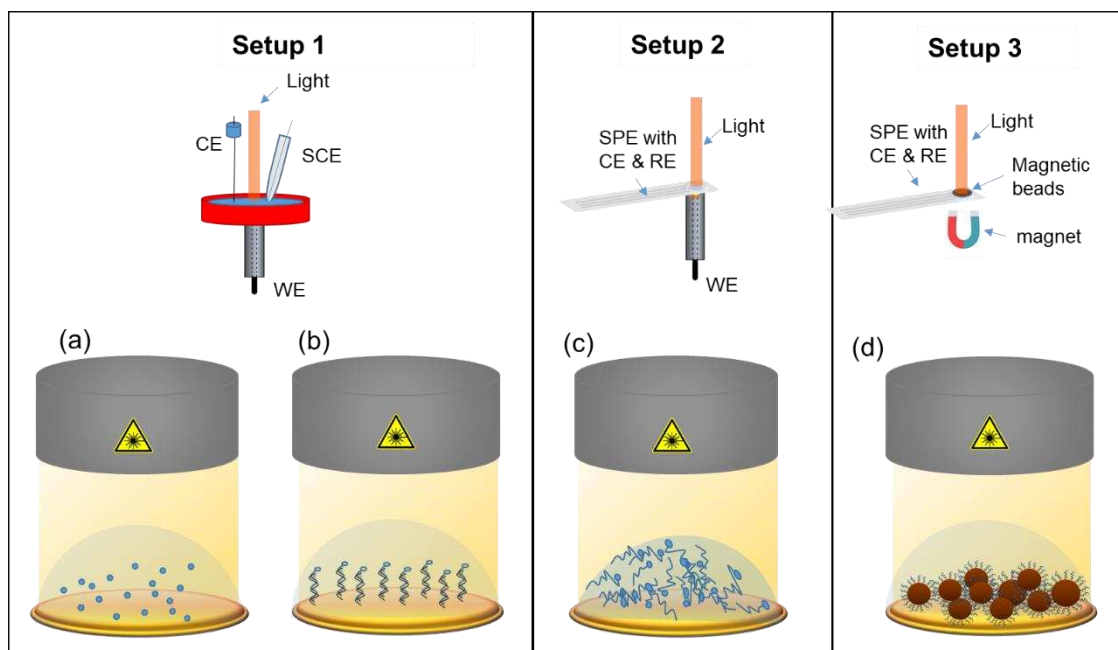
Figure 2. Representation of three photoelectrochemical setups used for four conditions in the study: (a) free chromophore dissolved in solution, (b) labeled DNA captured at the surface of the gold electrode, (c) labeled DNA dissolved in solution and (d) labeled DNA is captured at the surface of magnetic beads. WE- working electrode, RE- reference electrode, CE- counter electrode.

Setup 3 was used for photoelectrochemical measurements with magnetic beads accumulated on the surface of a gold-sputtered planar electrode (AUTR10, Dropsens) by placing a neodymium magnet underneath. As an alternative, carbon screen printed electrodes (C-SPE, Dropsens) were tested in the same manner. Before the measurements, beads were re-suspended in 10 µL of phosphate buffer and gently transferred into the measuring drop, where all the beads quickly precipitated at the working electrode due to a neodymium magnet below it. Photocurrents in this setup were measured at -0.15 V vs. the SPE quasi reference electrode (100 ± 5 mV vs. SCE).

All chronoamperometric photoelectrochemical measurements were conducted in light-chopped conditions (10 s or 30 s ON and 60 s OFF). Polynomial baseline correction was constructed through background current values (in dark) and subtracted from the amperograms to obtain baseline-corrected photocurrent responses. For ease of visual comparison among the electrodes, all the amperograms were plotted after subtraction of the baseline.

7

2.5. Spectroscopic measurements

An Implen NanoPhotometer N60 (Implen GmbH, Germany) was used to measure the UV-Vis spectra of labeled DNA. AvaSpec-2048 L from Avantes equipped with an AvaLight-DH-S-BAL light source was used to record the UV-Vis spectra of chromophores. The $^1O_2$ -producing capability of free chromophores was assessed with UV-VIS spectroscopy in the measuring buffer used for photoelectrochemical studies. Furfuryl alcohol (FFA, 98 %, J&K Scientific) was used as a chemical trap to detect and quantify the capability of the chromophores to generate $^1O_2$ (Appiani et al. 2017; Haag et al. 1984; Kochevar and Redmond 2000). The UV-vis spectra (in the range of 210 — 1000 nm) along with the time label were recorded automatically every 20 s under continuous stirring and illumination with a corresponding laser adjusted to 30 mW. The changes in the absorbance region of [FFA-O_2] formation at 240 nm were monitored for 16 minutes. The relative ability of the chromophores to produce $^1O_2$ was then calculated after correction with photon flux for the three light sources. The kinetics were normalized to the absorbance factor (1-$10^{-absorbance}$) at the laser wavelength for accurate correlation with the $^1O_2$ quantum yields (Φ_Δ), although the concentrations of the dyes were initially adjusted to provide similar absorbance in solution. The measurements were repeated at least three times.

3. Results and discussion

3.1 Photoelectrochemical detection of light-responsive DNA probes

Most of the organic chromophores that are used for DNA labeling (so-called light-responsive probes) can be categorized into three general groups: fluorescent chromophores that do not induce chemical reactions, photosensitizers that produce radicals upon light radiation but do not form $^1O_2$ (so-called type I photosensitizers) and photosensitizers that produce $^1O_2$ (so-called type II photosensitizers). However, some chromophores can exhibit mixed behavior. For example, some photosensitizers show mixed type I and II behavior (Abe et al. 1997; Núñez Montoya et al. 2005). Many photosensitizers also show fluorescence whereas many well-known fluorophores can generate small amounts of ROS (Gandin et al. 1983). We chose a series of chromophores of different types that are commercially available in forms ready for coupling to oligonucleotides giving us the light-responsive DNA probes. We expect those chromophores acting as type I and type II photosensitizers should produce noticeable photocurrent (Trashin et al. 2017; Zhao et al. 2014a) and, thus, should be useful as molecular labels in photoelectrochemical DNA sensors. In contrast, fluorescent dyes without photosensitizing properties should not generate a noticeable photocurrent. The near zero potential of -0.05 V providing a high

8

absolute current and a high signal/blank ratio (Fig. S1) was chosen as the potential for performing chronoamperometry.
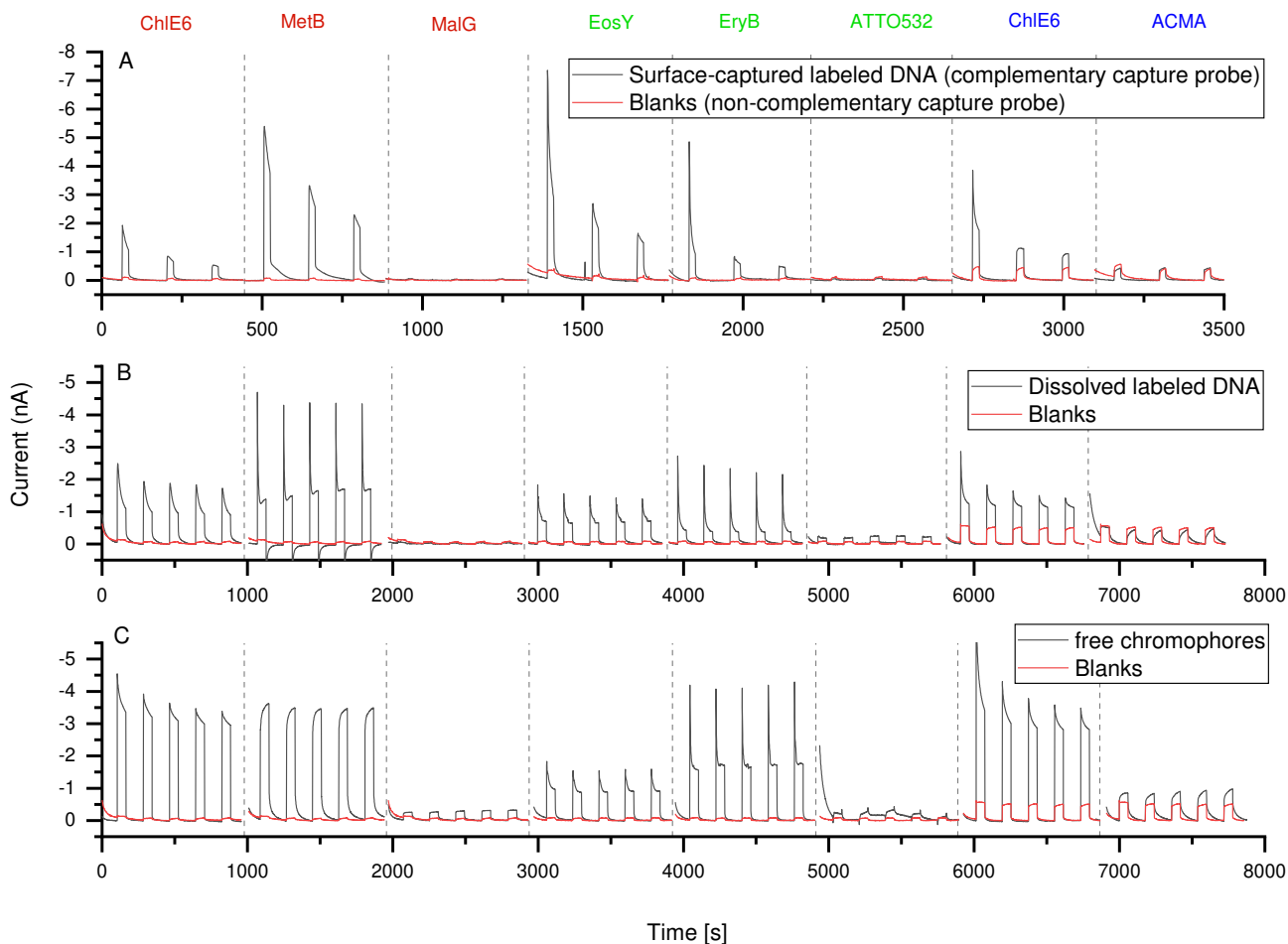
Figure 3. Chronoamperograms under chopped-light conditions for (A) surface-captured labeled DNA hybridized to complementary capture probe immobilized to gold electrode surface via thiol, in comparison to blanks from a non-complementary capture probe, (B) 5 µM dissolved labeled DNA in solution on, (C) 5 µM free chromophores in solution, on gold electrodes. The blanks in (B) and (C) were obtained in pure phosphate buffer. The electrodes were illuminated with the LED lasers (659 nm for ChlE6, MetB, MalG; 532 nm for EosY, EryB, ATTO532; 406 nm for ChlE6, ACMA) with an output power of 30 mW and a spot diameter adjusted to ca. 4 mm.

Fig. 3A shows the light chopped chronoamperograms of light-responsive DNA probes, labeled with seven different chromophores after captured by the surface-confined complementary capture DNA probe at the electrode surface (attached to the surface via the thiol group). An identical electrode with non-

complementary (scrambled) DNA probes was used as a blank control and showed only diminishing photocurrent responses. Well-known type II photosensitizers chlorin e6 (ChlE6) and methylene blue (MetB) showed strong photocurrent responses for the complementary strands. Whereas a well-known type I photosensitizer malachite green (MalG) (Wojtovich and Foster 2014) showed no photocurrent responses. Moreover, familiar fluorescent dye ATTO 532 (structurally similar to rhodamine 6G) and 9-amino-2-methoxy-6-chloroacridine (ACMA), gave no photocurrent responses for the complementary strand either. In contrast, eosin Y (EosY) and erythrosine B (EryB), containing the same xanthene core as ATTO 532 but exhibiting well-documented type II photosensitizing behavior (Gandin et al. 1983), showed clear photocurrent responses in the same conditions. From this, we conclude that the type II photosensitizing mechanism is essential for chromophores to generate a photocurrent in the taken conditions, presumably due to the electrochemical reduction of $^1O_2$ at the applied potential of -0.05 V vs SCE.

Interestingly, the photocurrent response decays rapidly during the illuminations and drops with each new illumination as shown in Fig. 3A. For example, in the case of EosY, the photocurrent dropped twice during the first illumination (10 s) and counted only 40% and 20% by the end of the second and the third illuminations, respectively. The same behavior was observed previously for an oligonucleotide labeled by pheophorbide a (Trashin et al. 2017) and we attributed this behavior to DNA cleavages by ROS without more detailed investigation. To discriminate between photobleaching of the chromophore and possible cleavages in the surface-confined duplex with the labeled DNA sequences, the labeled DNA, as well as the chromophores in the free form, were tested as dissolved in the buffer using the same electrodes but without any capture DNA-probe immobilized on the gold surface. In these conditions, only photobleaching can result in photocurrent decay whereas cleavages, even if happened, should not change the concentration and activity of the chromophore. Indeed, in contrast to the surface-captured labeled DNA, the responses for dissolved species were essentially repeatable over a sequence of at least three illuminations (Fig. 3B and C). This confirms that the chromophores are stable in the used conditions at least within the experimental time. Thus, the signal decay for the surface-confined chromophores as in Fig. 3A indeed results from the DNA cleavages from the gold surface followed by diffusion of the labeled fragments away from the electrode surface.

3.2 Correlation of photocurrents with optical properties and $^1O_2$ quantum yields of chromophores

Surface-captured DNA, dissolved labeled DNA and free chromophores showed generally similar reactivity profiles for each chromophore (Fig. 3). Also, some specific features can be identified and

10

attributed to the difference in extinction coefficients at the corresponding laser wavelengths (Fig. S2). In particular, EosY gives a higher photocurrent compared to EryB when linked to DNA and opposite in the free form (Fig. 3B and C). This behavior is explained by a shift in positions of the absorbance maxima in linked chromophores compared to the free chromophores (Table 1, Fig. S3 and S4), possibly due to changes in the microenvironment or shifts in pKa of dyes linked to DNA (Sjöback et al. 1998). This shift affects the extinction coefficient at 532 nm for EosY and EryB in such a way that the ratio between them reverses in the free form (Table 1). This confirms that the photoelectrochemical activity of the chromophores correlates with their extinction coefficients.

In addition, the extinction coefficient for MetB-DNA at 659 nm is 6 times higher compared to that of ChlE6-DNA, which explains a higher photocurrent for MetB-DNA compared to ChlE6-DNA although the $^1O_2$ quantum yield is expected to be higher for ChlE6 (Fernandez et al. 1997; Spikes and Bommer 1993). The extinction coefficient for MetB in free form is only 2.7 times higher than that of ChlE6. Besides, MetB may dimerize in water (Ghanadzadeh et al. 2008; Shahinyan et al. 2019), which was evident in our conditions from the UV-vis spectra that showed an increase of absorbance in the shoulder at 620 nm (Fig. S4). The dimerization is known to suppress $^1O_2$ quantum yields, which, along with the smaller difference in the extinction coefficients, explains the change in the relative activity of MetB in comparison to ChlE6. Surprisingly, the change of the laser wavelength from 659 to 406 nm, where ChlE6 has 5 times higher extinction coefficient, does not improve the photocurrent. This might be related to a stronger engagement of the chromophore in secondary photoreactions when excited into a more energetic electronic state and noticeable formation of superoxide radical, a known $^1O_2$ quencher (Guiraud and Foote 1976).

Table 1. Extinction coefficients ε ($M^{-1}cm^{-1}$) at given wavelengths λ (nm) for the chromophore linked to DNA and in the free form.

	Chromophore linked to DNA				Free chromophore			
	λ_{max}	$\varepsilon(\lambda_{max})$	λ_{laser}	$\varepsilon(\lambda_{laser})$	λ_{max}	$\varepsilon(\lambda_{max})$	λ_{laser}	$\varepsilon(\lambda_{laser})$
ChlE6	645	2.3E+04	659	1.2E+04	656	4.8E+04	659	4.3E+04
MetB	673	8.8E+04	659	7.6E+04	665	1.1E+05	659	1.1E+05
MalG	626	7.2E+04	659	2.2E+04	622	7.0E+04	659	1.3E-04
EosY	524	8.6E+04	532	7.0E+04	517	1.3E+05	532	5.4E+04
EryB	537	4.8E+04	532	4.6E+04	524	1.0E+05	532	8.6E+04
ATTO532	534	1.1E+05	532	1.1E+05	534	1.4E+05	532	1.3E+05

ChlE6	410	1.4E+05	406	1.4E+05	403	2.3E+05	406	2.2E+05
ACMA	645	2.3E+04	406	1.2E+04	425	1.3E+04	406	8.5E+03

Because of the clear link between the type II photosensitization mechanism and the registered photocurrent, we assessed the relative $^1O_2$ quantum yields of the used chromophores in our experimental conditions employing an independent method, i.e. the spectrophotometric monitoring of furfuryl alcohol (FFA) as $^1O_2$ trap. The measurements were conducted with the same lasers and the buffer as in the chronoamperometric experiments. The relative activity of the photosensitizers was obtained from the accumulation kinetics for the [FFA-O$_2$] adduct under constant light illumination (Table 2). The spectra of the chromophores before and after the illumination, changes in the region of 240 nm and the kinetics of accumulation of FFA-O$_2$ adduct in comparison with blank recorded in the absence of FFA are presented in detail in the supplementary information (Figure S5-S7). As expected, the type II photosensitizers (MetB, ChlE6, EosY and EryB) resulted in the comparatively fast accumulation of the FFA-O$_2$ adduct, whereas other dyes showed minor or no formation of FFA-O$_2$ (Table 2). In particular, this confirms that MalG does not generate any significant amount of $^1O_2$ while ACMA and ATTO532 have very minor $^1O_2$ generation (30 times lower than for ChlE6) which corresponded to the complete absence of the photocurrent for MalG with still very minor photocurrents for ACMA and ATTO532. Additionally, MalG degrades noticeably, faster than other compounds used in this study (Fig. S8), via type I reaction, undergoing $OH^{\bullet}$, $O_2^{\bullet-}$ and H^+ mediated photocatalytic degradation (Ray et al. 2018). The highest activity was obtained for EosY, which is, in combination with a high extinction coefficient at 532 nm when linked to DNA (7.0E+04 $M^{-1}cm^{-1}$) resulted in the highest photocurrent. MetB, in agreement with the evident dimerization, showed a 2 times lower production of $^1O_2$ compared to EosY in the same conditions (Table 2). However, DNA-linked MetB does not suffer from this limitation, which explains its high photoelectrochemical activity in Figures 3A and B compared to EosY.

Table 2. Relative $^1O_2$ production ability of free chromophores in each wavelength region of light.

	Concentration* (µM)	Relative kinetics for [FFA-O$_2$] formation	Literature $^1O_2$ quantum yields (Φ_Δ)
ChlE6	5.0	1.00 ± 0.02	0.71 (Redmond and Gamlin 1999), 0.64 (Fernandez et al. 1997), 0.66 (Spikes and Bommer 1993)
MetB	2.0	0.54 ± 0.01	0.52 (Fernandez et al. 1997), 0.60 (Redmond and Gamlin 1999), 0.49 (Lutkus et al. 2019)

MalG	40	-0.002 ± 0.002	<0.003 (Wojtovich and Foster 2014)
EosY	5.0	1.31 ± 0.09	0.52, 0.57 (Redmond and Gamlin 1999), 0.61 (Lutkus et al. 2019)
EryB	2.5	1.22 ± 0.04	0.68 (Redmond and Gamlin 1999) 0.62 (Pellosi et al. 2013)
ATTO532	2.0	0.03 ± 0.00	N/A (fluorescent (Glembockyte et al. 2016))
ChlE6	1.0	0.80 ± 0.03	0.71 (Redmond and Gamlin 1999), 0.64 (Fernandez et al. 1997), 0.66 (Spikes and Bommer 1993)
ACMA/ quinacrine	20	0.03 ± 0.01	0.013 (Motten et al. 1999; Valencia U et al. 2003)

* Concentrations were adjusted to get the same absorbance of 0.2 at the laser wavelengths.
**The kinetics of ChlE6 was taken as 1.

Noteworthy, quinacrine which is identical to ACMA linked to DNA showed only minor $^1O_2$ production (the $^1O_2$ quantum yield Φ_Δ ca. 3% is in agreement with previous literature (Motten et al. 1999; Valencia U et al. 2003)), although, the parent chromophore acridine is known as a good type II photosensitizer (Φ_Δ = 0.84 in benzene and 0.97 in acetonitrile (Scurlock and Ogilby 1993). Possibly, another acridine derivative can be used as a better type II photosensitizer with activity in the blue region of the visible spectrum. Thus, we established the strong link between the chromophore's ability to produce $^1O_2$ and the recorded photocurrents at -0.05 V vs SCE.

3.3 Enhancement of the photocurrent by the photocatalytic redox cycling

Considering the quick decay of the photocurrent in surface-captured probes and its comparatively overall low absolute values in all three situations (Fig. 3A, B & C), an enhancement strategy would be of high interest for the analytical application of the introduced system. Previously we found that, when reacting with singlet oxygen, HQ provides a fast, intense and stable photocurrent response without any electrode fouling at pH 7 (Trashin et al. 2017) making it an ideal model for electroactive $^1O_2$ quencher and the redox mediator in the system used. Moreover, HQ has a redox potential of -0.05 V vs SCE at pH 7, (Guo et al. 2019), whereas the most easily oxidized base guanine oxidizes only at + 0.7 V vs SCE (Ferapontova and Domínguez 2003). Though the difusion distance of $^1O_2$ is relatively short (< 100 nm), we made sure that the amount of HQ (10 μM) was always kept in excess in comparison to the concentration of photosensitizers in all the measurement conditons used in this study (Fig. 2) . This excess of HQ favorably reacts with $^1O_2$ and, thus, should protect DNA bases from oxidation and cleavages and transforms short-lived and highly reactive $^1O_2$ into a stable compound (BQ), electroactive at a given electrode and potential applied. Moreover, electrochemical reduction of benzoquinone (BQ) back into HQ which reacts again with $^1O_2$ forming the redox cycle.

Both surface-captured and dissolved labeled DNA were tested in the presence of 10 μM HQ (Table 3). Interestingly, the photocurrent dropped about twice in the case of type II chromophores linked DNA, captured at the electrode, but enhanced about 3-7 times for dissolved ones. This suppression can be explained by a comparatively slow overall kinetics of the transformation of HQ into BQ under the action of $^1O_2$ following a fast [2+4]-cycloaddition of $^1O_2$ with the formation of an endoperoxide (Lam et al. 2006). In other words, HQ rapidly quenches $^1O_2$ forming the intermediate but slowly forms the final redox-active product (BQ). In contrast, the direct reduction of $^1O_2$ at the electrode is expected to be fast. Thus, the use of HQ enhances the photocurrent only when $^1O_2$ is generated at some distance from the electrode so that $^1O_2$ cannot reach it due to the short lifetime (~3.5 μs in quencher-free H_2O). In the case of dissolved labeled DNAs, most of $^1O_2$ are generated in bulk and can result in a photocurrent only due to its reaction with HQ leading to BQ that produces photocurrent. Importantly, no noticeable photocurrent was observed in the presence of HQ for DNA labeled with the non-fluorescent photosensitizer MalG, fluorescent dye ATTO532, and ACMA. This confirms the essential role of $^1O_2$ in the scheme with the HQ/BQ redox cycle.

Table 3. Photocurrents (nA) at 10 s from the start of illuminations.

	λ_{laser}	Surface-captured labeled DNA		Dissolved labeled DNA	
		Pure buffer	In the presence 10 μM HQ	Pure buffer	In the presence 10 μM HQ
ChlE6	659	-1.36 ± 0.21	-0.55 ± 0.02	-1.39 ± 0.19	-6.63 ± 0.51
MetB	659	-3.45 ± 0.50	-0.37 ± 0.06	-1.99 ± 0.36	-3.23 ± 0.33
MalG	659	-0.02 ± 0.01	-0.02 ± 0.01	-0.05 ± 0.04	-0.04 ± 0.05
EosY	532	-1.74 ± 0.81	-0.2 ± 0.04	-1.69 ± 0.22	-7.10 ± 0.52
EryB	532	-1.26 ± 0.13	-0.18 ± 0.04	-0.99 ± 0.10	-7.44 ± 0.29
ATTO532	532	-0.08 ± 0.07	-0.14 ± 0.04	-0.06 ± 0.04	-0.11 ± 0.04
ChlE6	406	-1.30 ± 0.30	-0.36 ± 0.06	-1.43 ± 0.34	-5.18 ± 0.26
ACMA	406	-0.04 ± 0.07	-0.06 ± 0.02	-0.14 ± 0.05	-0.21 ± 0.08

The values are taken at 10 s (in the middle of an illumination cycle) from the moment of switching the light on to avoid the initial spikes in the photocurrent.

To further improve the sensitivity of the detection paradigm with HQ as redox reporter, the capture DNA was immobilized on magnetic beads (2.7 μm in diameter) instead of attaching capture DNA directly on the electrode. We chose DNA-ChlE6 (with the 659 nm red laser) and DNA-EryB (with the 532 nm green

laser) that showed the highest photocurrents in dissolved form in the presence of HQ. DNA-MalG and ATTO532-DNA were chosen as control in the respective region of light. A 406 nm blue laser was not considered for further study owing to its higher blank responses. The beads capturing the labeled DNA through hybridization were retained by a magnet below a working electrode. For this reason, planar gold-sputtered electrodes were used. The magnetic beads carry a much larger number of capture DNA probe than it would be present on the electrode surface (theoretical value *ca.* 150 pmol/cm^2 in case of magnetic beads compared to *ca.* 20 pmol/cm^2 in case of gold electrode surface (Steel et al. 2000; Thiruvottriyur Shanmugam et al. 2020) but keep the DNA above the electrode, in the layer which is few μm thick. Because of the distance, the photocurrent in absence of HQ is lower for the case of magnetic beads compared to DNA directly immobilized on gold electrodes, which is in agreement with the diffusion distance of $^1O_2$ (*ca.* 0.2 μm) limited by its lifetime. Noteworthy, only gold-sputtered planar electrodes were applicable for the measurements since the regular screen printed carbon electrodes showed high blank photocurrents (Fig. S11). Further optimization studies with different concentrations of HQ are warranted for improving the sensitivity of a given sensing application.

In the absence of HQ, only a minor photocurrent marginally higher than the blank photocurrent was registered after incubation with 50 nM complementary DNA labeled with the dyes. However, in the presence of HQ, the photocurrent response increased by 28 and 20 times for DNA-ChlE6 and DNA-EryB respectively (Fig. 4C). There was also signal decay observed for consecutive illuminations similar to surface-captured labeled DNA over consecutive illuminations due to the cleavage of labeled DNA probes from magnetic beads. When compared to the 4 and 7 folds increase for dissolved labeled DNA (Fig. 4B) and about twice the response drop for surface-captured DNA (Fig. 4A), thus suggesting that the usage of beads indeed enhances the analytical performance of the sensing strategy. The overall sensitivity of the sensing platform increased compared to gold disk electrodes by 56 times and the signal-to-blank ratio improved by 3 times for ChlE6 and 8 times for EryB. Moreover, the use of magnetic beads in combination with the disposable electrodes facilitated the workflow and allowed to conduct of a large test to evaluate the concentration and analytic performances (Fig. 5). As the result, the photocurrent increased proportionally with the concentration of the labeled DNA and presented a linear dynamic range of 250

pM- 25 nM and 50pM- 10 nM, detection limits of 17 pM and 10 pM and sensitivity of 116 A/M/cm^2 and 213 A/M/cm^2 were calculated for DNA-ChlE6 and DNA-EryB respectively.
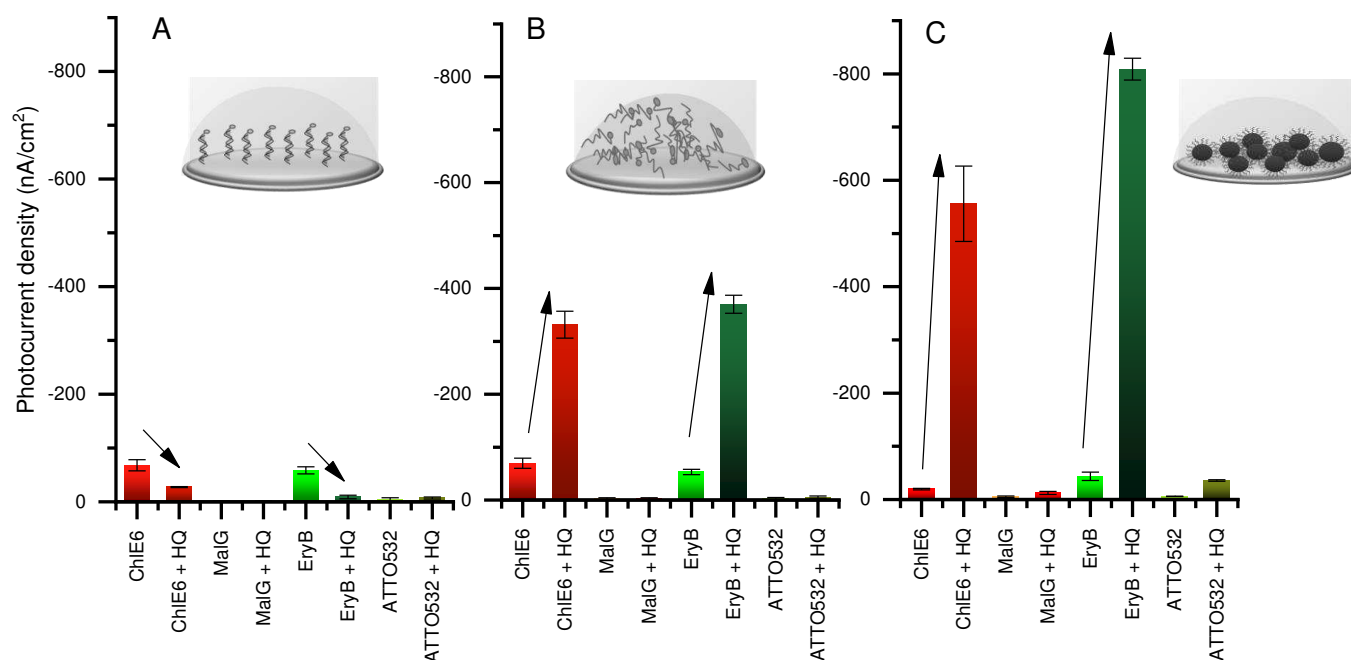
Figure 4. Comparison of photocurrent responses A- Surface-captured labeled DNA, B- dissolved labeled DNA and C- magnetic beads-captured labeled DNA, in the presence and absence of 10 µM HQ. Arrows indicate the increase/decrease of responses with HQ.

Noteworthy, the performances of MB as an electrochemical tag (normally applied in a different detection scheme as a "signal-off" sensor also called E-DNA) are well documented in the literature and can be compared with our assay (Kang et al. 2012; Kang et al. 2009; Kara et al. 2002; Rowe et al. 2011; Shen et al. 2012; Xiao et al. 2007). In the electrochemical scheme, a DNA probe with MB tag is attached to the surface and the formation of a duplex with a target DNA suppresses the voltammetric response of MB. The peak current in the voltammetric response of MB is around 200-500 nA and is generally consistent in the literature (Kang et al. 2012; Xiao et al. 2007). Our amperometric photocurrent on the same type of electrodes is only 3.5 nA (Fig. 3A), i.e. about 100-folds lower than the voltammetric peak current, but, with a good signal/noise ratio even for low absolute currents due to averaging of the signal over time. Furthermore, the use of magnetic beads and HQ as the redox reporter further amplifies the amplitude of our amperometric responses about 50x times (Fig. S12). More importantly, the electrochemistry of MB-tagged DNA is extremely sensitive to the distance between the tag and the electrode. Indeed, MB shows no SWV peak when the labeled DNA molecules are captured by the magnetic beads and placed on the electrode (Fig. S12 A) due to no actual contact between MB and the electrode. However, the photocurrent of (240 ±20) nA was measured in the same conditions in the presence of 10 uM HQ as the redox reporter to capture singlet oxygen (Fig. S12 B). This is advantageous compared to the use of MB as an electrochemical tag.

16
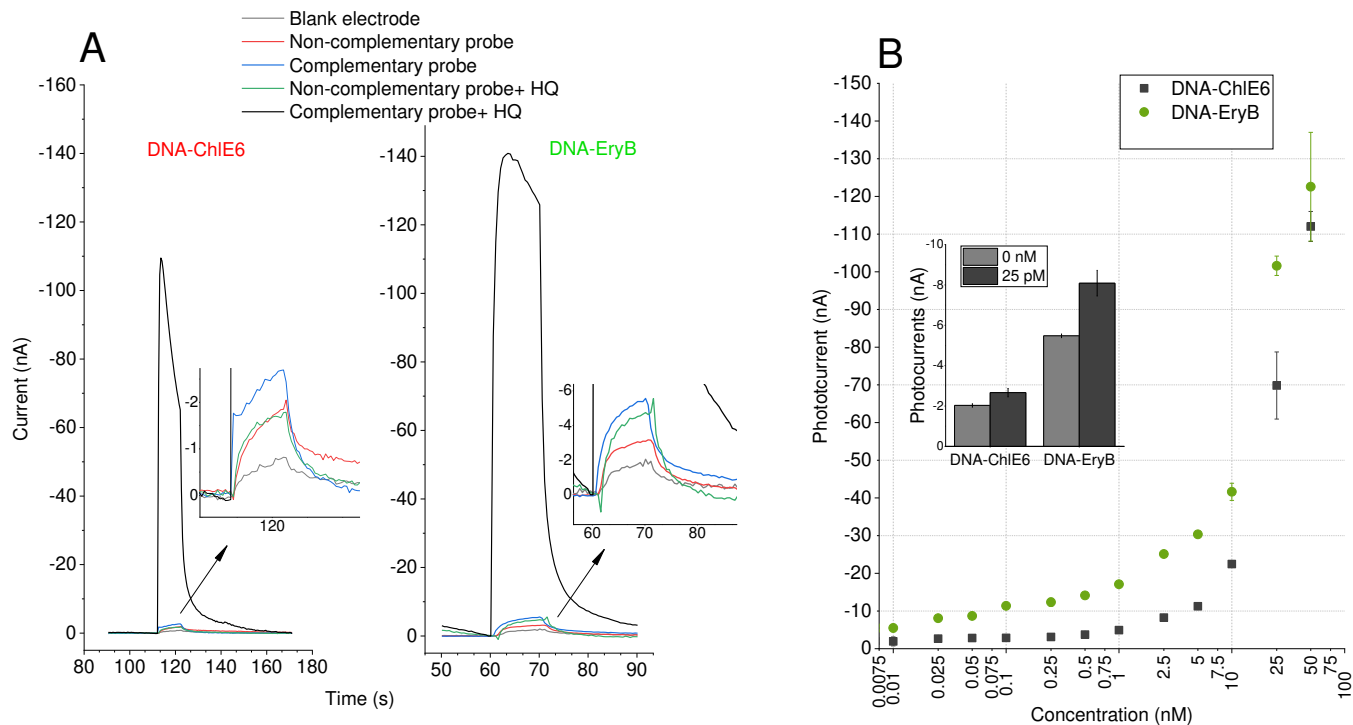
Figure 5 A- Chronoamperograms from magnetic beads-captured labeled DNA probes (50 nM) with chlorin e6 and erythrosine, after incubation with complementary and non-complementary capture probes attached to magnetic beads. B- Chronoamperometric detection of different concentrations of DNA-CE6 and DNA-Ery using the magnetic beads-based photoelectrochemical platform.

4. Conclusion

We assessed a novel photoelectrochemical DNA sensing strategy based on the ability of type II molecular photosensitizers to produce $^1O_2$. Noticeable photoelectrochemical responses in nanoampere (nA) ranges were obtained for type II photosensitizers but only negligible photocurrents were observed for type I photosensitizer (malachite green) and fluorescent dye ATTO432 (structure close to Rhodamine 6G) and ACMA (structure close to quinacrine). The use of the 406 nm blue laser was associated with increased photocurrent in blanks compared to the 532 nm green and the 659 nm red lasers, making the last two to be preferred ones in applications. The photoelectrochemical activity of the tested dyes correlated well with the ability to produce $^1O_2$ and optical properties of the chromophores. Further enhancement of the photocurrent was achieved by using hydroquinone as a redox reporter for chemical capturing of short-lived $^1O_2$ in few micrometers thick layers of magnetic beads attracted to a planar disposable electrode by a magnet.

17

Successful demonstration of the analytical performance using a disposable platform provides a foundation for novel electrochemical sensors that use photocatalysts analogous to enzymatic catalysts and fluorescent labels but avoid the drawbacks of enzymatic sensors such as poor stability of enzymes. This study was limited by several commercially available ready-to-use labels, while much more efficient type II photosensitizers are available and can be synthetically customized for attachment to DNA. The dyes having the absorbance maxima all over the visible light range open the perspective for multiplexed sensing of different target DNA/RNA sequences simultaneously.

Acknowledgments

Appendix A. Supplementary data

Reference

Abe, H., Ikebuchi, K., Wagner, S.J., Kuwabara, M., Kamo, N., Sekiguchi, S., 1997. Photochem Photobiol 66(2), 204-208.
Appiani, E., Ossola, R., Latch, D.E., Erickson, P.R., McNeill, K., 2017. Environ Sci Process Impacts 19(4), 507-516.
Bhargava, A., Kumar Khare, N., Bunkar, N., Chaudhury, K., Chand Pandey, K., K. Jain, S., K. Mishra, P., 2017. Current Pharmaceutical Design 23(8), 1175-1187.
Bronkhorst, A.J., Ungerer, V., Holdenrieder, S., 2020. Critical Reviews in Clinical Laboratory Sciences 57(4), 253-269.
Demchenko, A.P., 2020. Methods Appl Fluoresc 8(2), 022001.
Ferapontova, E.E., 2018. Annu Rev Anal Chem (Palo Alto Calif) 11(1), 197-218.
Ferapontova, E.E., Domínguez, E., 2003. Electroanalysis 15(7), 629-634.
Fernandez, J.M., Bilgin, M.D., Grossweiner, L.I., 1997. Journal of Photochemistry and Photobiology B: Biology 37(1), 131-140.
Gandin, E., Lion, Y., Van de Vorst, A., 1983. Photochemistry and Photobiology 37(3), 271-278.
García-González, R., Costa-García, A., Fernández-Abedul, M.T., 2014. Sens Actuators B Chem 191, 784-790.
Ghanadzadeh, A., Zeini, A., Kashef, A., Moghadam, M., 2008. Journal of Molecular Liquids 138(1), 100-106.
Glembockyte, V., Lin, J., Cosa, G., 2016. The Journal of Physical Chemistry B 120(46), 11923-11929.
Guiraud, H.J., Foote, C.S., 1976. Journal of the American Chemical Society 98(7), 1984-1986.
Guo, Y., He, D., Xie, A., Qu, W., Tang, Y., Zhou, L., Zhu, R., 2019. Polymers 11(11), 1907.
Haag, W.R., Hoigne´, J.r., Gassman, E., Braun, A.M., 1984. Chemosphere 13(5), 631-640.
Horaková-Brazdilova, P., Fojtova, M., Vytras, K., Fojta, M., 2008. Sensors (Basel) 8(1), 193-210.
Islam, M.N., Moriam, S., Umer, M., Phan, H.-P., Salomon, C., Kline, R., Nguyen, N.-T., Shiddiky, M.J.A., 2018. Analyst 143(13), 3021-3028.

Kang, D., White, R.J., Xia, F., Zuo, X., Vallée-Bélisle, A., Plaxco, K.W., 2012. NPG Asia Materials 4(1), e1-e1.

Kang, D., Zuo, X., Yang, R., Xia, F., Plaxco, K.W., White, R.J., 2009. Analytical Chemistry 81(21), 9109-9113.

Kara, P., Kerman, K., Ozkan, D., Meric, B., Erdem, A., Nielsen, P.E., Ozsoz, M., 2002. Electroanalysis 14(24), 1685-1690.

Kim, H.-s., Abbas, N., Shin, S., 2021. Biosensors and Bioelectronics 177, 113005.

Kochevar, I.E., Redmond, R.W., 2000. [2] Photosensitized production of singlet oxygen. Methods in Enzymology, pp. 20-28. Academic Press.

Kokkinos, C., 2019. Nanomaterials 9(10), 1361.

Lam, W.W.Y., Lee, M.F.W., Lau, T.-C., 2006. Inorganic Chemistry 45(1), 315-321.

Li, Y., Sthal, C., Bai, J., Liu, X., Anderson, G., Fang, Y., 2021. Journal of Virological Methods 289, 114040.

Liu, X.P., Chen, J.S., Mao, C.J., Niu, H.L., Song, J.M., Jin, B.K., 2018. Biosens Bioelectron 116, 23-29.

Liu, Z.-J., Yang, L.-Y., Wei, Q.-X., Ye, C.-L., Xu, X.-W., Zhong, G.-X., Zheng, Y.-J., Chen, J.-Y., Lin, X.-H., Liu, A.-L., 2020. Talanta 216, 120966.

Lutkus, L.V., Rickenbach, S.S., McCormick, T.M., 2019. Journal of Photochemistry and Photobiology A: Chemistry 378, 131-135.

Malatesta, M., Giagnacovo, M., Costanzo, M., Conti, B., Genta, I., Dorati, R., Galimberti, V., Biggiogera, M., Zancanaro, C., 2012. Eur J Histochem 56(2), e20-e20.

Motten, A.G., Martínez, L.J., Holt, N., Sik, R.H., Reszka, K., Chignell, C.F., Tonnesen, H.H., Roberts, J.E., 1999. Photochem Photobiol 69(3), 282-287.

Niemz, A., Ferguson, T.M., Boyle, D.S., 2011. Trends in Biotechnology 29(5), 240-250.

Núñez Montoya, S.C., Comini, L.R., Sarmiento, M., Becerra, C., Albesa, I., Argüello, G.A., Cabrera, J.L., 2005. Journal of Photochemistry and Photobiology B: Biology 78(1), 77-83.

Pellosi, D.S., Batistela, V.R., Souza, V.R.d., Scarminio, I.S., Caetano, W., Hioka, N., 2013. Anais da Academia Brasileira de Ciências 85, 1267-1274.

Rahat, B., Ali, T., Sapehia, D., Mahajan, A., Kaur, J., 2020. Frontiers in Genetics 11(844).

Rashid, J.I.A., Yusof, N.A., 2017. Sensing and Bio-Sensing Research 16, 19-31.

Ray, S.K., Dhakal, D., Lee, S.W., 2018. Photochem Photobiol 94(3), 552-563.

Redmond, R.W., Gamlin, J.N., 1999. Photochem Photobiol 70(4), 391-475.

Rowe, A.A., Bonham, A.J., White, R.J., Zimmer, M.P., Yadgar, R.J., Hobza, T.M., Honea, J.W., Ben-Yaacov, I., Plaxco, K.W., 2011. PLOS ONE 6(9), e23783.

Santhanam, M., Algov, I., Alfonta, L., 2020. Sensors 20(16), 4648.

Scurlock, R.D., Ogilby, P.R., 1993. Journal of Photochemistry and Photobiology A: Chemistry 72(1), 1-7.

Sfragano, P.S., Pillozzi, S., Palchetti, I., 2021. Electrochemistry Communications 124, 106929.

Shahinyan, G.A., Amirbekyan, A.Y., Markarian, S.A., 2019. Spectrochimica Acta Part A: Molecular and Biomolecular Spectroscopy 217, 170-175.

Shen, Z., Nakayama, S., Semancik, S., Sintim, H.O., 2012. Chemical Communications 48(61), 7580-7582.

Sjöback, R., Nygren, J., Kubista, M., 1998. Biopolymers 46(7), 445-453.

Spikes, J.D., Bommer, J.C., 1993. Journal of Photochemistry and Photobiology B: Biology 17(2), 135-143.

Steel, A.B., Levicky, R.L., Herne, T.M., Tarlov, M.J., 2000. Biophysical Journal 79(2), 975-981.

Tavallaie, R., De Almeida, S.R., Gooding, J.J., 2015. Wiley Interdiscip Rev Nanomed Nanobiotechnol 7(4), 580-592.

Thiruvottriyur Shanmugam, S., Trashin, S., De Wael, K., 2020. Analyst 145(23), 7646-7653.

Tokudome, H., Yamada, Y., Sonezaki, S., Ishikawa, H., Bekki, M., Kanehira, K., Miyauchi, M., 2005. Applied Physics Letters 87(21).

Trashin, S., Rahemi, V., Ramji, K., Neven, L., Gorun, S.M., De Wael, K., 2017. Nature Communications 8(1).

19

Valencia U, C., Lemp, E., L. Zanocco, A., 2003. Journal of the Chilean Chemical Society 48, 17-21.

Victorious, A., Saha, S., Pandey, R., Soleymani, L., 2021. Angewandte Chemie International Edition 60(13), 7316-7322.

Wang, M., Yin, H., Shen, N., Xu, Z., Sun, B., Ai, S., 2014. Biosens Bioelectron 53, 232-237.

Wang, Q., Zhang, H., Shen, X., Wang, F., Mao, C., 2020. ChemistrySelect 5(48), 15259-15263.

Wojtovich, A.P., Foster, T.H., 2014. Redox Biol 2, 368-376.

Xiao, Y., Qu, X., Plaxco, K.W., Heeger, A.J., 2007. Journal of the American Chemical Society 129(39), 11896-11897.

Zhao, W.-W., Xu, J.-J., Chen, H.-Y., 2014a. Chemical Reviews 114(15), 7421-7441.

Zhao, W.W., Xu, J.J., Chen, H.Y., 2014b. Chem Rev 114(15), 7421-7441.

Supplementary information

Singlet oxygen-based photoelectrochemical detection of DNA

Saranya Thiruvottriyur Shanmugam[a, b], Stanislav Trashin[a, b], Karolien De Wael[a, b*]

[a]A-Sense Lab, Department of Bioengineering, University of Antwerp, Groenenborgerlaan 171, 2020 Antwerp, Belgium.

[b]NANOlab Center of Excellence, University of Antwerp, Groenenborgerlaan 171, 2020 Antwerp, Belgium

[*]Corresponding author, karolien.dewael@uantwerpen.be

Table of contents

1. Optimization of the potential for amperometry

A

B

Figure S1: A- Effect of potential (vs SCE) on the specific photoelectrochemical response from 5 µM photosensitizer and the blank buffer response in PB, pH7 on GDE. B- Signal to noise ratio of photosensitizer and blank buffer as function of potential. Error bars indicate measurements from different electrodes.

2. UV-Vis spectra of diode lasers used in this study
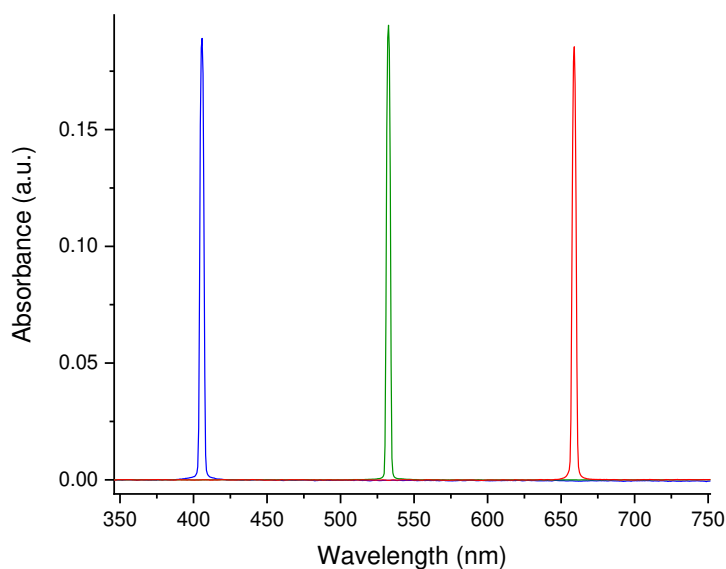
Figure S2 UV-Vis spectra of 3 diode lasers (405 nm- blue, 532 nm- green, 659 nm – red) irradiating the phosphate buffer used in this study.
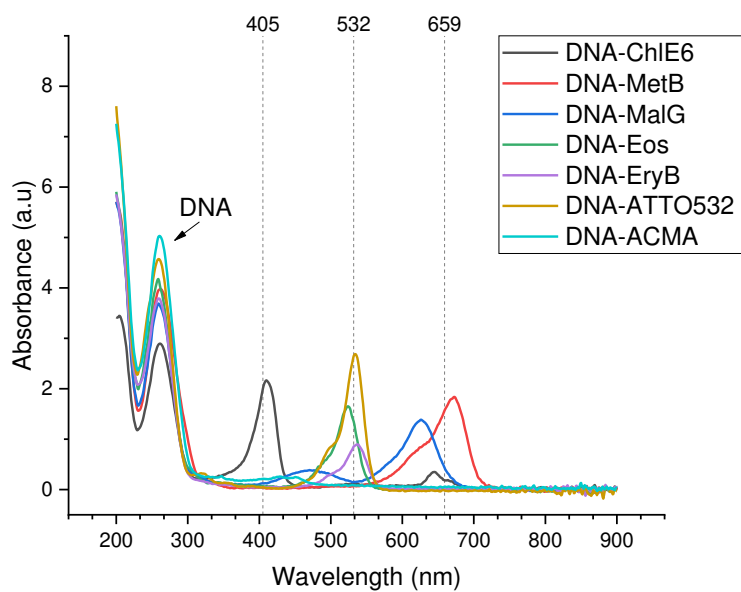
Figure S3 UV-Vis spectra of 20 µM chromophores-DNA in measuring buffer, PB, pH 7. The vertical reference lines indicate the wavelengths of lasers used in this study.
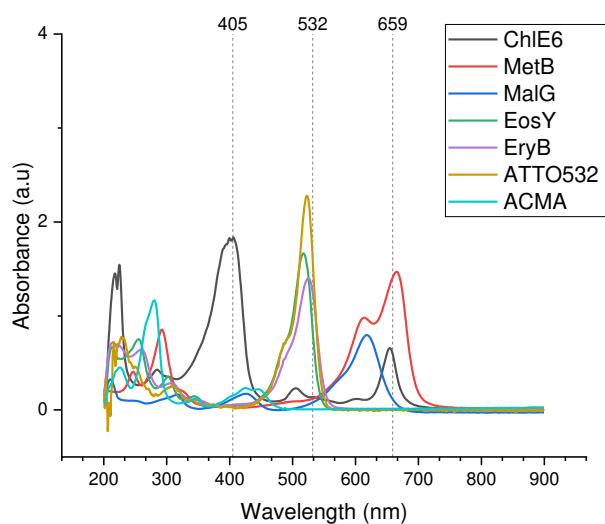
Figure S4 UV-Vis spectra of 20 µM chromophores in measuring buffer, PB, pH 7. The vertical reference lines indicate the wavelengths of lasers used in this study.

2. Estimation of relative kinetics for formation FFA-O₂

MetB

ChlE6

MalG
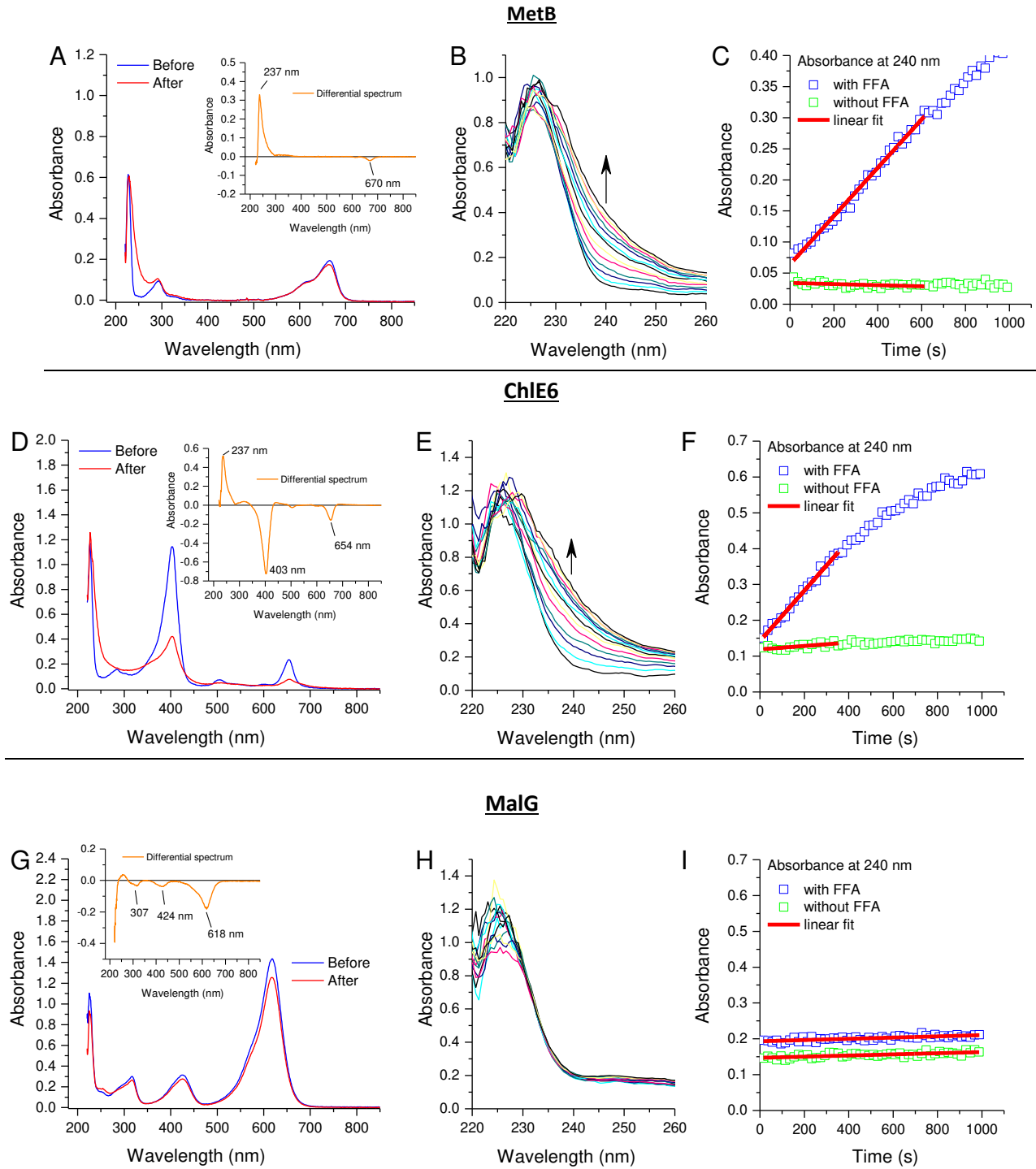
Figure S5 The spectra of chromophores before and after illumination with the red 659 nm laser for 16 min (A, D, G), changes in the region of 240 nm (B, E, H) and the kinetics of accumulation of FFA-O₂ adduct in comparison with blank recorded in the absence of FFA (C, F, I).
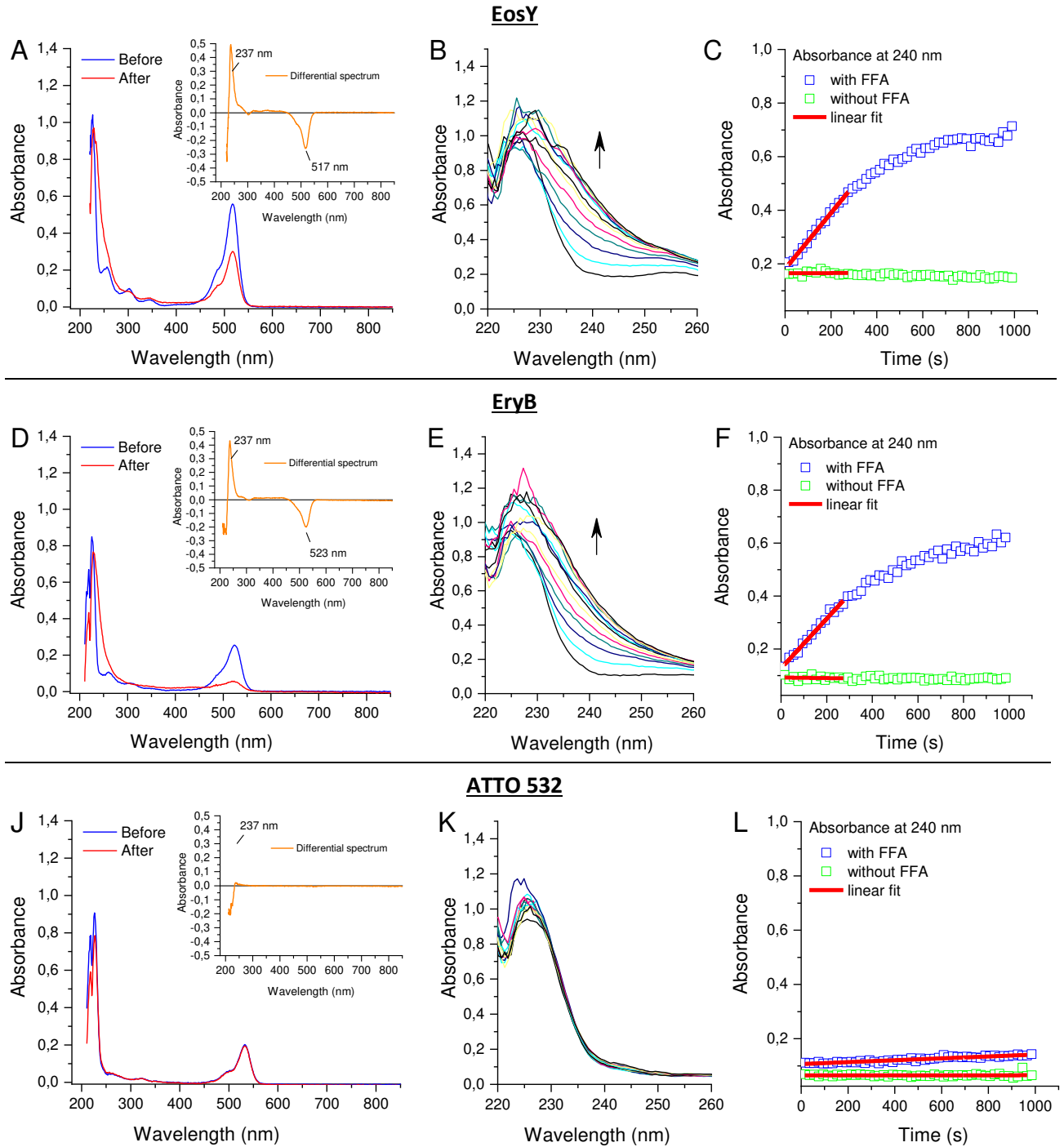
Figure S6 The spectra of chromophores before and after illumination with the green 532 nm laser for 16 min (A, D, J), changes in the region of 240 nm (B, E, K) and the kinetics of accumulation of FFA-O_2 adduct in comparison with blank recorded in the absence of FFA (C, F, L).

ChlE6

ACMA (quinacrine)
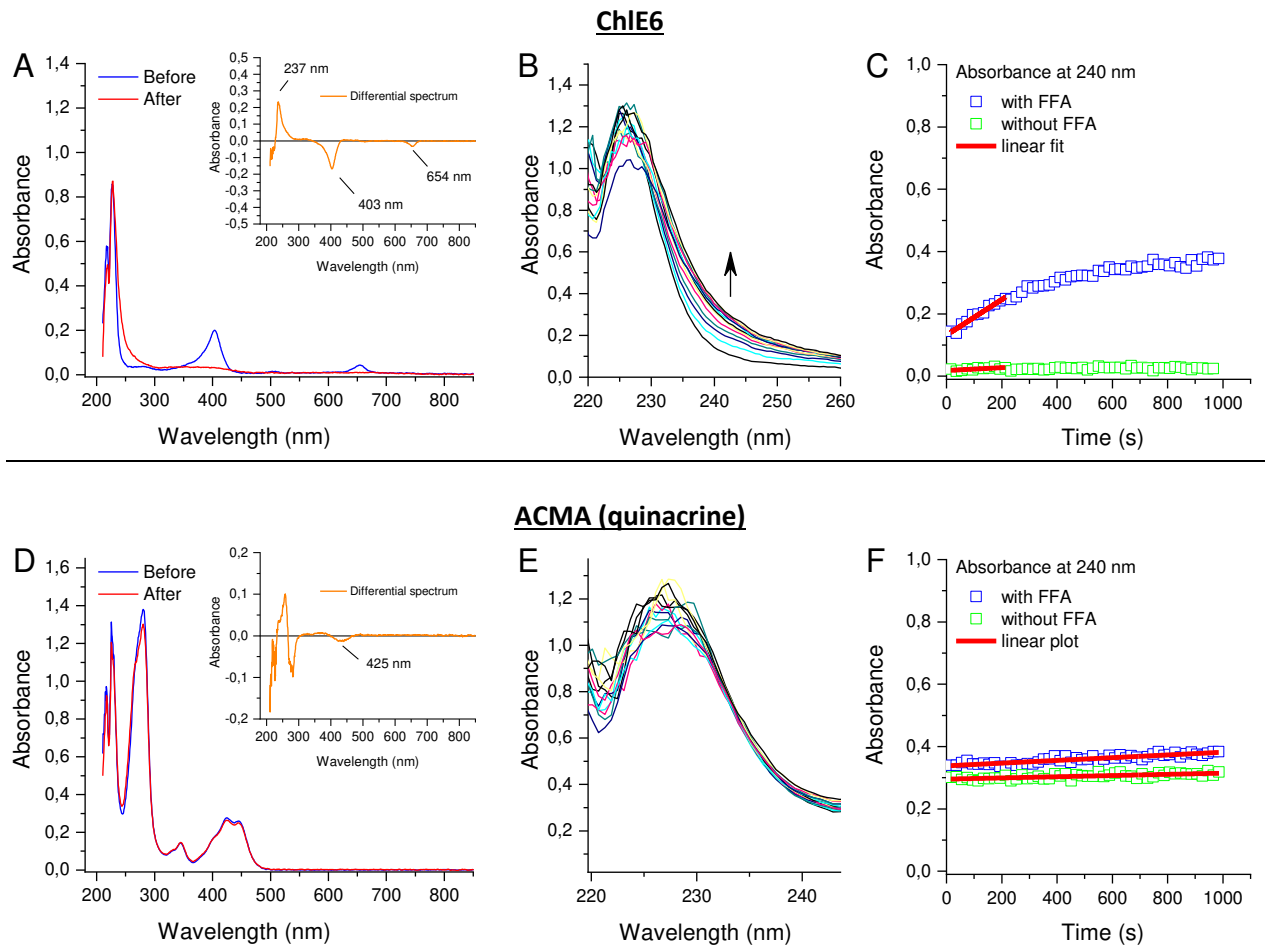
Figure S7 The spectra of chromophores before and after illumination with the green 406 nm laser for 16 min (A, D, G, J), changes in the region of 240 nm (B, E, H, K) and the kinetics of accumulation of FFA-O_2 adduct in comparison with blank recorded in the absence of FFA (C, F, I, L).

3. Results from photodegradation kinetics without FFA

MetB

ChlE6

MalG
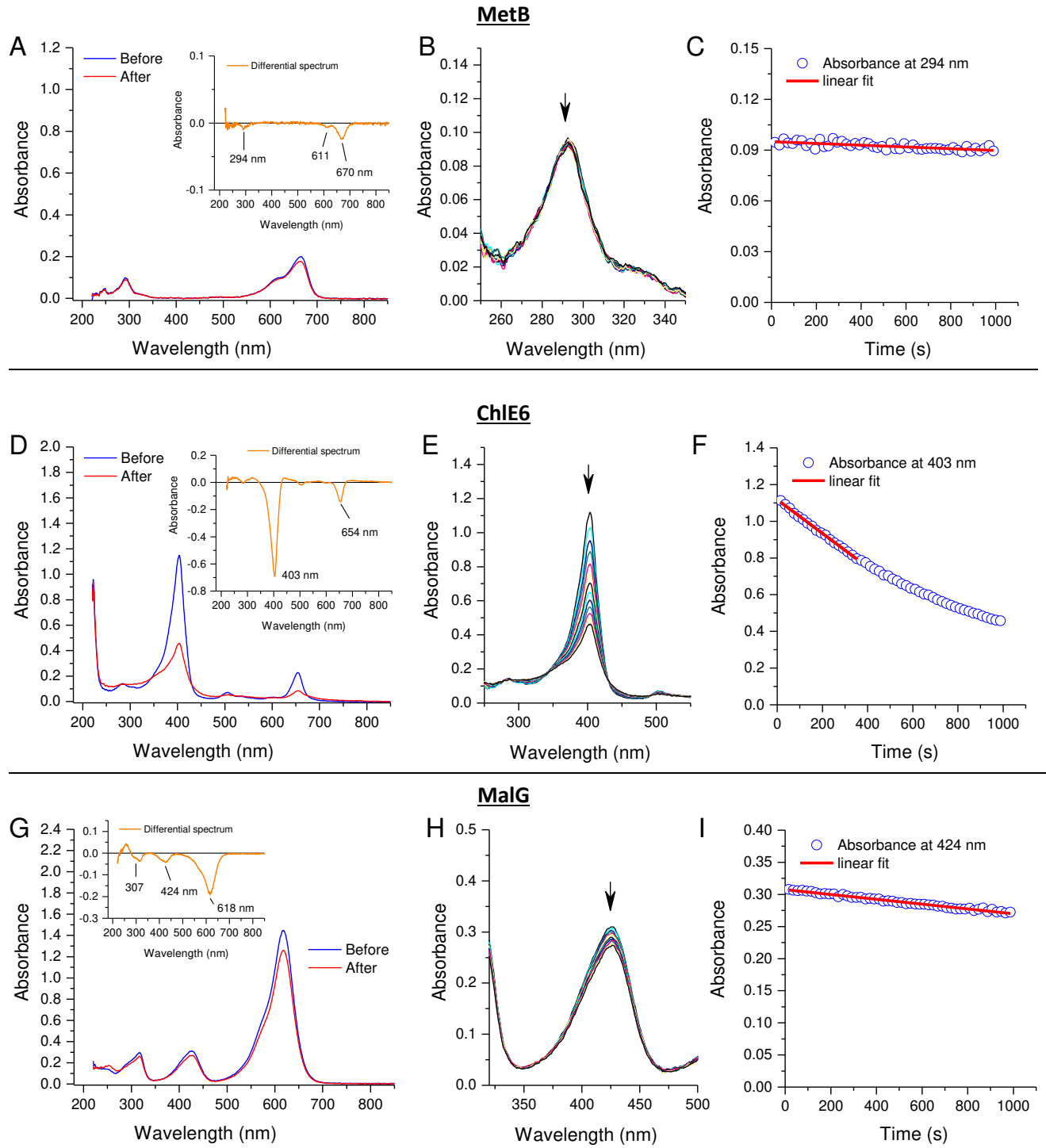
Figure S8 The spectra of the chromophores before and after illumination with the red 659 nm laser for 16 min (A, D, G), changes in the region of one of the absorbance maxima (B, E, H) and the kinetics of the changes (C, F, I).
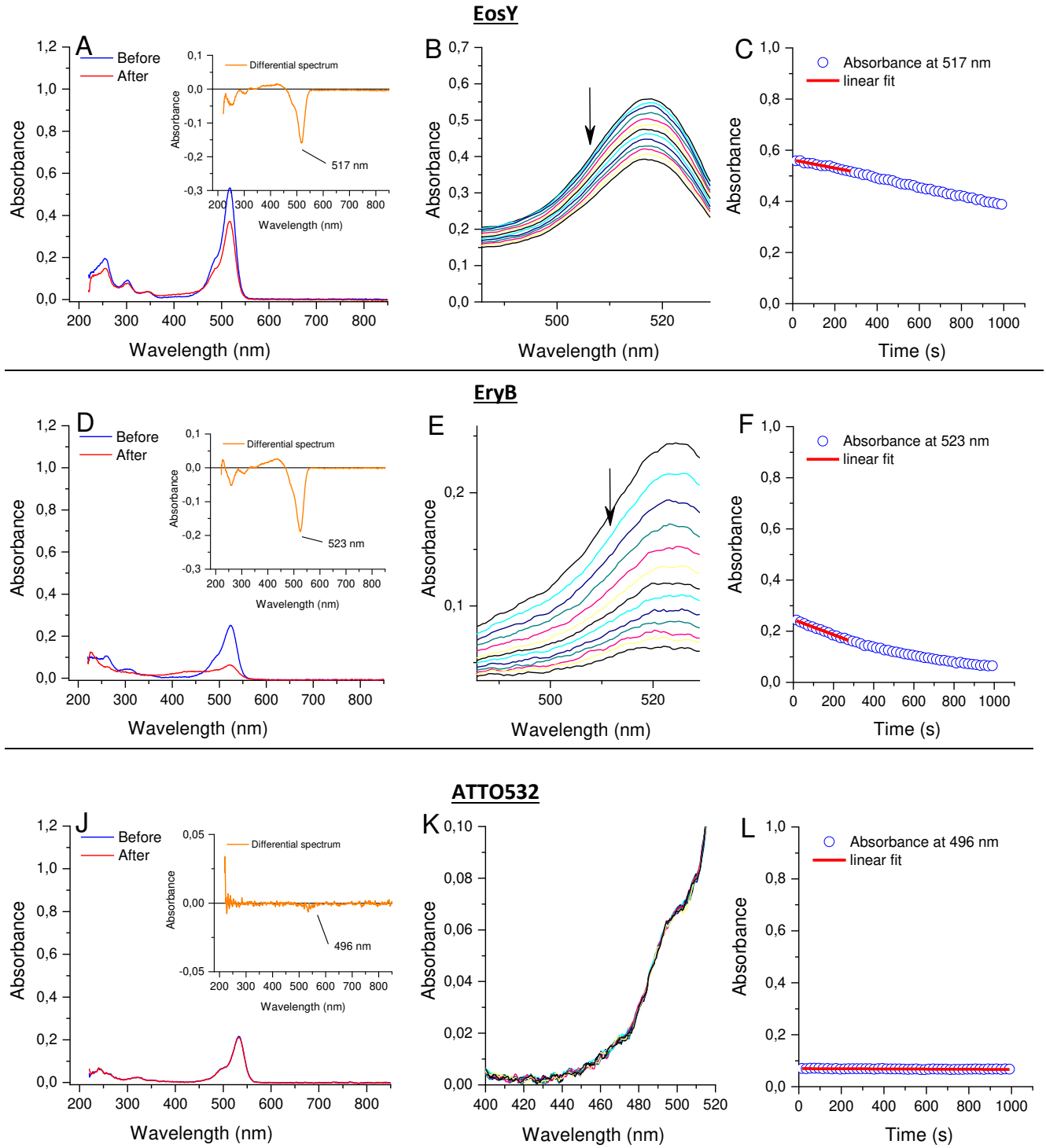
Figure S9 The spectra of the chromophores before and after illumination with the green 532 nm laser for 16 min (A, D, J), changes in the region of one of the absorbance maxima (B, E, K) and the kinetics of the changes (C, F, L).

ChlE6

ACMA
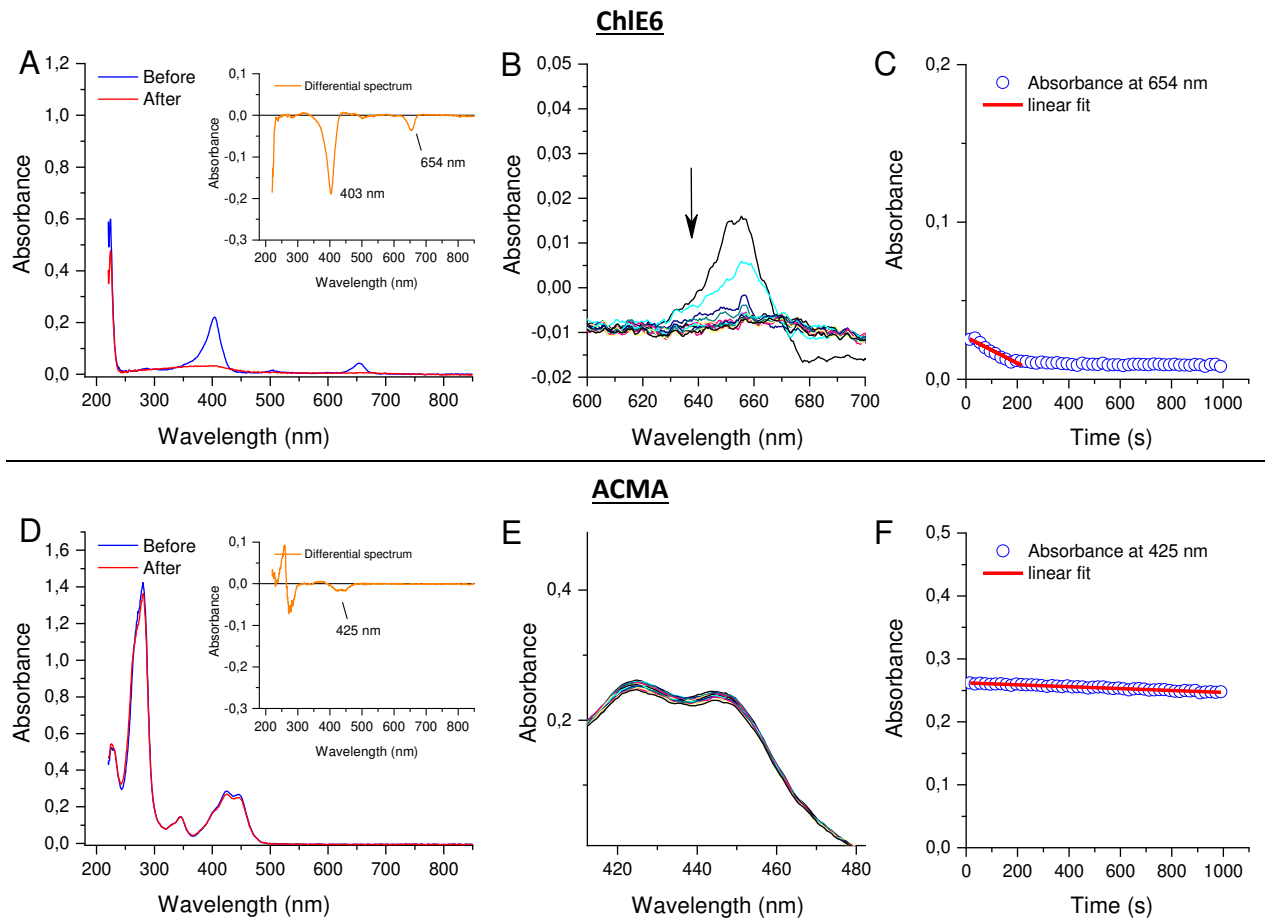
Figure S10 The spectra of the chromophores before and after illumination with the blue 406 nm laser for 16 min (A, D), changes in the region of one of the absorbance maxima (B, E) and the kinetics of the changes (C, F).

4. Photocurrent responses from free chromophores in the absence and presence of hydroquinone

Table 1 Photocurrents (nA) at 10 s from the start of illuminations for 5 μM of free chromophores.

	Pure buffer	In the presence of 10 μM HQ
ChlE6	-3.27 ± 0.20	-10.07 ± 0.60
MetB	-2.47 ± 0.40	-13.67 ± 0.80
MalG	-0.14 ± 0.05	-0.36 ± 0.02
EosY	-1.03 ± 0.30	-8.13 ± 0.30
EryB	-2.83 ± 0.10	-8.73 ± 0.20
ATTO532	-0.09 ± 0.06	-0.53 ± 0.11
ChlE6	-2.98 ± 0.60	-10.66 ± 0.40
ACMA	-0.28 ± 0.06	-0.78 ± 0.07

5. Screen-printed electrodes for magnetic beads assay

Carbon screen printed electrodes (C-SPE) that are easy to handle and with no prerequisite of pretreatment or cleaning were initially chosen simplifying the sensor preparation. The beads, with a monolayer of streptavidin covalently coupled to the surface, were bound to biotinylated DNA and hybridized with the labelled DNA and dropped on the working electrode surface. Neodymium magnets (placed beneath the electrode) concentrated the magnetic beads at the surface of the working electrode, also facilitating improvement in the sensitivity. Under these conditions, the distance between the chromophore and the surface is much larger than the distance $^1O_2$ can diffuse during its lifetime (200 nm), thus the current is mostly due to the reaction of $^1O_2$ with HQ contributing to the HQ-BQ redox cycle. Figure S7 (left) shows the responses obtained for 50 nM DNA-ChlE6 hybridized on beads in the presence and absence of HQ at C-SPE at 659nm. It can be seen that a low photocurrent response is obtained for DNA-ChlE6 beads similar to the blank photocurrents. No noticeable change or very minor increase in the photocurrent was observed when HQ was present in the measuring conditions. Noisy signals with no noticeable photocurrents from the chromophores are due to the high background bias from the carbon working surface of the SPE. Thus, another disposable platform was chosen that would have a gold working electrode surface mimicking the pure gold surface of a gold disk electrode and also has practical applicability of SPEs to place magnets beneath the working surface of the electrode. Figure S7 (right) presents the blank responses from a red laser at Au-SSPE compared to C-SPE and GDE. The baseline current of Au-SSPE (~20 nA) is much smaller compared to C-SPE (~100 nA) and much closer to GDE (usually in the range of 5-10 pA) comparatively. This indirectly suggests that the evenness and purity of the electrode surface is in the following order: GDE>Au-SSPE>>C-SPE. Therefore, Au-SSPE was chosen for further measurements with magnetic beads.
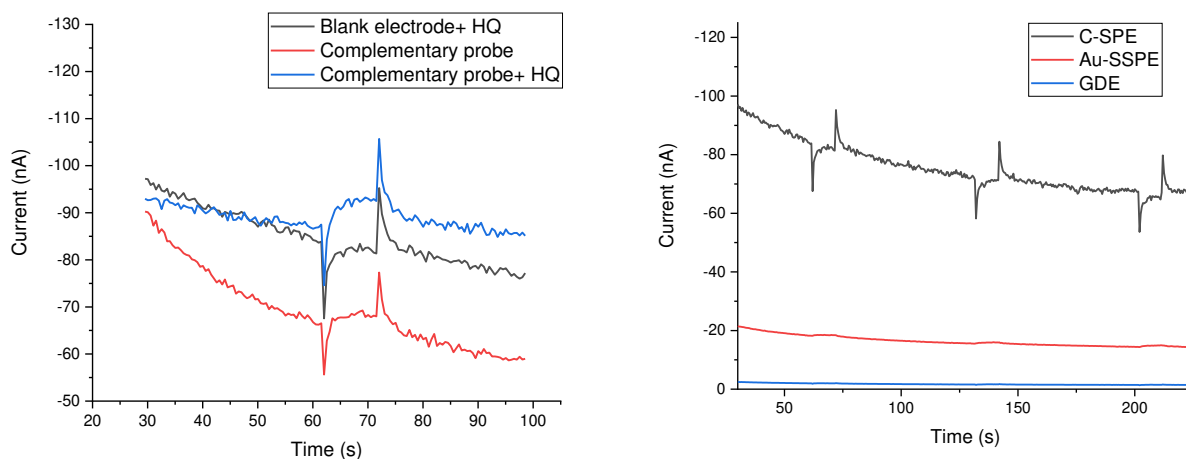
Figure S11 Left- Chronoamperoograms presenting the photocurrent response of 50 nM labeled DNA captured on magnetic beads. Blank electrode denotes the response from the gold surface without any beads only containing 10 μM HQ in the buffer. Right- Blank responses from C- SPE, Au- SSPE, and GDE without any beads. Amperometry was performed at -0.15 V vs internal pseudo Ag reference in PB pH7 using a red (659 nm) laser.
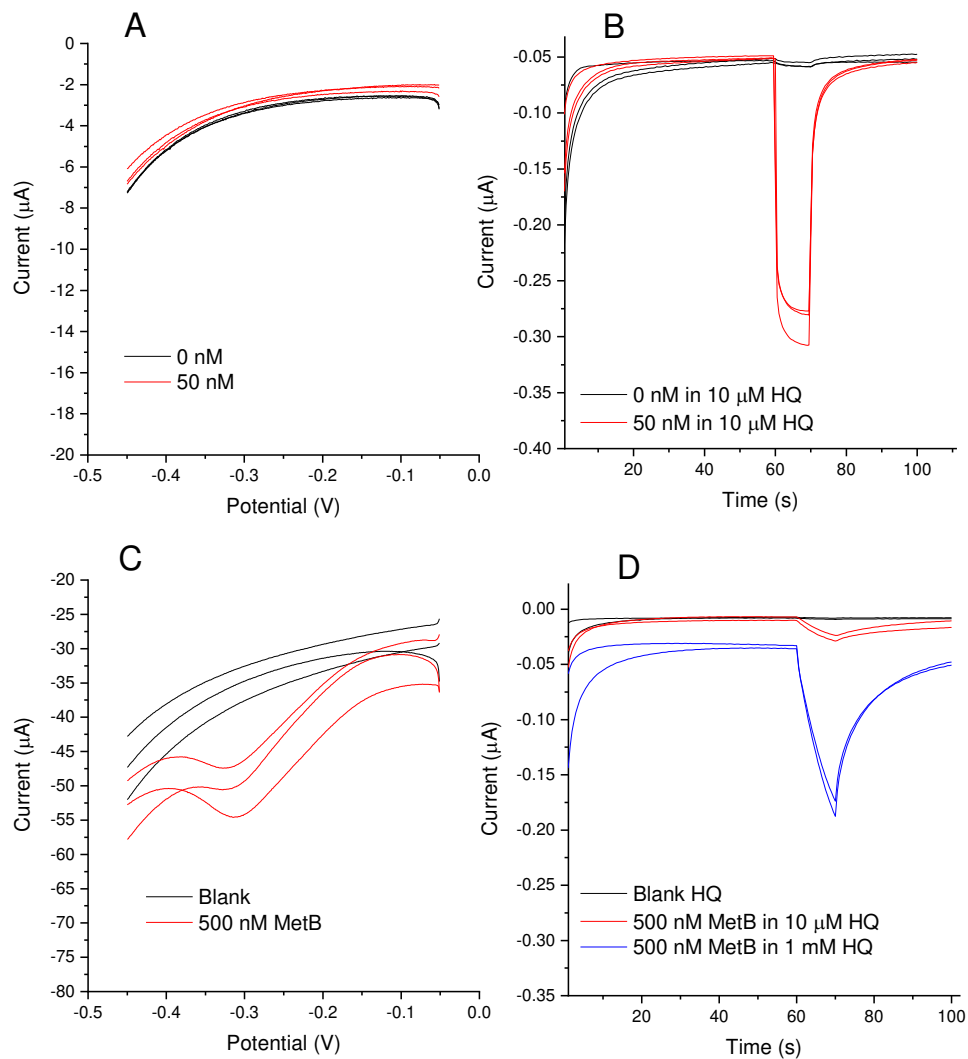
Figure S12: (A) Square wave voltammetric (SWV behavior of magnetic beads after incubation in 50 nM target DNA labeled with MetB in comparison to the blank. SW amplitude = 75 mW, frequency 100 Hz, scan rate: 100 mV/s. Measuring buffer, 0.1 M KCl, 0.01 M KH₂PO₄ pH 7. (B) the photocurrent response of magnetic beads in the presence of 10 μM HQ after incubation in 50 nM target DNA labeled with MetB in comparison to the blank. Illumination with the 659 nm red diode laser, 30 mW. Measuring buffer, 0.1 M KCl, 0.01 M KH₂PO₄ pH 7. (C) SWV response of 0.5 μM MetB demonstrating the expected peak position for MetB in the conditions of measurements with labeled DNA. (D) the photocurrent response of 0.5 μM MetB in the presence of 10 μM HQ, same conditions as in (B).